In situ tomographic observation of dendritic growth in Mg/Al matrix composites

Enyu Guo, A.B. Phillion, Zongning Chen, Huijun Kang, Tongmin Wang, Peter D Lee

Abstract

Understanding the interaction of nano/micro-particles with evolving microstructures during solidification is critical for developing new materials with improved mechanical properties through either particulate reinforcement and/or via microstructural refinement. In this study, we investigate the influence of nanoparticles on the evolving dendrites in both Mg and Al based metal matrix composites via *in situ* synchrotron tomography. Ultrasonic treatment was applied during the raw material preparation to break the particle agglomeration. The solidification of primary dendrites was characterized and quantified. The results reveal the underlying physical mechanisms that enable nanoparticles to modify the grain size in both alloy systems. These insights into dendrite evolution help both to inform and validate numerical models of the solidification microstructures of metal matrix composites.

Keywords

Metal matrix composites; microstructural evolution; dendrite; nanoparticles; tomography

---

E. Guo *, Zongning Chen, Huijun Kang, Tongmin Wang
Key Laboratory of Solidification Control and Digital Preparation Technology (Liaoning Province), School of Materials Science and Engineering, Dalian University of Technology, Dalian, 116024, China
*email (E. Guo): eyguo@dlut.edu.cn; Tel: +44-(0)411-84709500

A.B. Phillion
Department of Materials Science and Engineering, McMaster University, Hamilton, L8S 4L7, Canada

Peter D Lee
Mechanical Engineering, University College London, WC1E 7JE, UK

1. Introduction

Particulate reinforced metal matrix composites (MMCs) can achieve better physical properties, e.g. higher specific strength, than metallic materials alone. Both micron and nanometre sized particulates are thought to introduce Orowan strengthening and/or grain refinement effects, bringing about improved mechanical performance [1-4]. Therefore, these MMC's have become important material candidates for ground transport and aerospace applications [1]. Ceramic micron-sized particles of Al_2O_3, SiC and TiB_2 have been used in MMC's [5-7], whilst nanoparticles such as SiC, Al_2O_3, TiB_2, Y_2O_3 and AlN are important reinforcements for metal matrix nano-composites (MMNCs) [2].

Liquid melt processing offers an economic way to fabricate the MMCs since the particles have the opportunity to control the evolution of the solidifying microstructure and thus the in-service mechanical properties of parts. One study reported that the dendrite's surface was modified after solidification when nano-particles (NPs) were added in the matrix [8]. Other studies revealed that particles ahead of the solid/liquid interface can be pushed or engulfed, depending on many factors including the dendrite growth velocity, particle size, interfacial energy, and particle thermal properties [9-11].

Direct observations of the evolving microstructures during solidification enable scientists and engineers to understand the influence of particles on the microstructure, and thus enabling the examination of the interacting mechanisms between the particles and the evolving microstructure. This is now readily available with the development of the 3rd generation synchrotron X-ray characterization techniques, especially the 3D (or even 4D, 3D plus time) tomography technique where the complex 3D morphology of the microstructures can be revealed in real time [12-15]. For example, the time evolved synchrotron tomography was used to study the effect of nanoparticles on solidification microstructures in Al alloys to reveal dendrite growth mechanisms in fcc crystal structures in the presence of NP's [16].

In a recent study, we investigated the influence of SiC nano-sized particles (NP) on the nucleation and growth of dendrites in a set of Mg-Zn-Al alloys using *in-situ* synchrotron X-ray tomography [17]. In this study, those results are extended and compared to experiments performed on Al-Cu alloys with and without nano/micron-sized particles (MP). The effect of particles on the dendritic growth is examined at low cooling rates, 2-3 ^{o}C/min. The difference in dendrite nucleation,

growth, and morphology is compared and discussed in the particle-free and MP/NP conditions. Note that these experiments are designed to study the microstructural evolution under the influence of NP or MP, and not to directly observe the particles themselves.

2. Experimental

2.1 Raw Materials

Magnesium alloys of Mg-25Zn-7Al (in wt.%) without and with ~0.7wt.% SiC NPs (ca. 40nm) and aluminum alloys of Al-10Cu (in wt.%) without and with ~1.0wt.% Al_2O_3 nano (ca. 50nm) or ~1.0wt.% Al_2O_3 micro (ca. 10 μm) particles were used for the solidification studies. The magnesium alloys were prepared by alloying an AZ91D (or AZ91D containing 1wt.% SiC NP) alloy with a Zn ingot (99.9%) in a steel crucible, melting under argon gas protection, casting into a preheated steel mold, and then machining cylindrical samples of Φ~1.2 mm for the synchrotron solidification experiments. The particle-containing Al-10Cu alloys were prepared from a master alloy and a 10 vol.% particle-containing alloy. Ultrasonic treatment was applied for ~5 min to both NP-containing alloys (ca. 1 kg) at ~50-100 ºC above the liquidus temperature of the alloys to disperse the NPs. The ultrasonic processing was performed using a titanium sonotrode under an ultrasonic wave of 3 kW power and frequency of 20 kHz. The ultrasonic treatment was not applied to the NP-free alloys. For the magnesium alloys, the samples were encapsulated following the method described in ref. [12].

2.2 *In situ* synchrotron solidification experiments

The *in situ* solidification experiments of magnesium alloys and aluminum alloys were carried out at the Diamond-Manchester Beamline (I13-2) of the Diamond Light Source (DLS, U.K) and the TOMCAT beamline of Swiss Light Source (SLS, Swiss), respectively. During each experiment, the sample was heated up to ~ 30 ºC above the liquidus temperature, held at that temperature for 10-20 min, and then cooled to induce solidification. The prescribed cooling rate was 3 ºC/min for the magnesium alloys and 2 ºC/min for the aluminum alloys.

The tomographic data of magnesium alloys were recorded during solidification using a pink beam (energy range 15-30 keV), and an imaging system composed of a PCO Edge 5.5 CMOS camera, and a single crystal $CdWO_4$ scintillator, resulting in 1.6 μm/pixel. Each dataset contained 1200 projections with an exposure time of 12 ms, resulting in a scan time of 14.4 s. Note however, that the scan-to-scan cycle time was 36 s (corresponding to 1.8 ºC) due to a time delay needed for

system re-initialization. The tomographic data of Al-10Cu alloys were recorded using a monochromatic beam (energy 35.6 keV) and a PCO Edge 5.5 camera that resulted in the resolution of 1.7 μm/pixel. Each tomographic scan contained 1800 projections and took ~33 s to complete the data collection.

The data of magnesium alloys were preprocessed following the method described in ref. [18] to minimize ring artefacts and improve phase contrast, while filtered back projection reconstruction was used for the Al-10Cu datasets. After data reconstruction and pre-processing, the primary dendrites were segmented using a global threshold value. The data was further analysed using the Image J and Avizo@ (Thermo Fisher Scientific, USA) software tools.

3. Results and discussion

3.1 2D microstructure evolution in Mg-25Zn-7Al alloys

Fig. 2 presents the overall microstructural evolution in the longitudinal slices at different temperatures for the NP-free and NP-containing Mg-25Zn-7Al alloys. A few observations can be made based on the slices. First, it is seen that the morphology of the dendrites is equiaxed for both the NP-free and NP-containing alloys. This is because the dendrites grew in all directions after nucleation due to the relatively heterogeneous temperature gradient within the melt. However, the shape of the NP-free grains appears to be dendritic, while the shape of the NP grains appears to be more globular. Second, the general size of α-Mg grains in NP-free Mg-25Zn-7Al, Fig. 1(a-c), was larger than in NP Mg-25Zn-7Al, Fig. 1(d-f). Thus, a significantly finer solidification microstructure was achieved after the addition of SiC NPs, indicating enhanced grain nucleation. Finally, the α-Mg dendrites appear to have nucleated heterogeneously, either on the oxide skin of the sample or on pre-existing pores (black regions in Fig. 1) within the melt (which most likely have oxides at their surface).

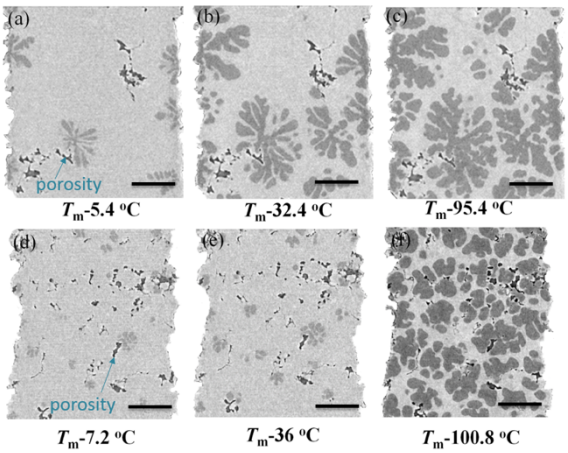

Fig. 1 Longitudinal slices showing the dendritic structures of NP-free Mg-25Zn-7Al (a-c) and NP Mg-25Zn-7Al (d-f) alloys solidified at 3 °C/min cooling rate. The temperature is indicated below each figure. Note, T_m denotes the melt temperature immediately prior to the first nucleation of solid. Scale bar in each figure is 300 μm. (Figures (a-c) are after ref. [17] (E. Guo et al. Acta Mater. 2018)

3.2 2D microstructure evolution in Al-10Cu alloys

Fig. 2 shows the evolution of solidification microstructures in an Al-10Cu alloy for three conditions: 1. without any particulate additions (Fig. 2a-d); 2. with Al_2O_3-nano-particulate (Fig. 2e-h); and 3. with micron-sized Al_2O_3 particulate (Fig. 2i-l). Comparing the three samples, it is clear that the addition of MP's has the largest effect on reducing grain size, e.g. Fig. 2(c) vs Fig. 2(k). This is interesting as it would be expected that nano particles might be expected to have a stronger growth restriction effect than micron sized particles [4]; however, Greer et al. hypothesized that larger particles are more effective at nucleation [19], a conclusion these results seem to support. Interestingly, the addition of both NP and MPs to the melt seems to reduce the amount of porosity formed. This could be due to several reasons: 1. the ultrasonic treatment used to process the Al_2O_3 containing melts included a degassing operation [20]; 2. the refinement of the microstructure also refines and reduces porosity [21]. Overall, however, it appears that the effect of Al_2O_3 particles, either micron or nano-sized on the solidification structure of Al-10Cu was less significant in refining the grain structure as compared to that of the SiC NPs in the Mg-25Zn-7Al.

The effect of particulate additions on the rate of coarsening of the secondary dendrite arms may be seen qualitatively by comparting the zoomed microstructures in Fig. 2. The secondary arm spacing is almost halved by the addition of NPs, and interestingly even further refined by the addition of MPs. This slowing of the coarsening of the microstructure during solidification has been

hypothesized to be due to the restriction of solute diffusion [10] – these results suggest that there is a similar effect for micron sized particles.

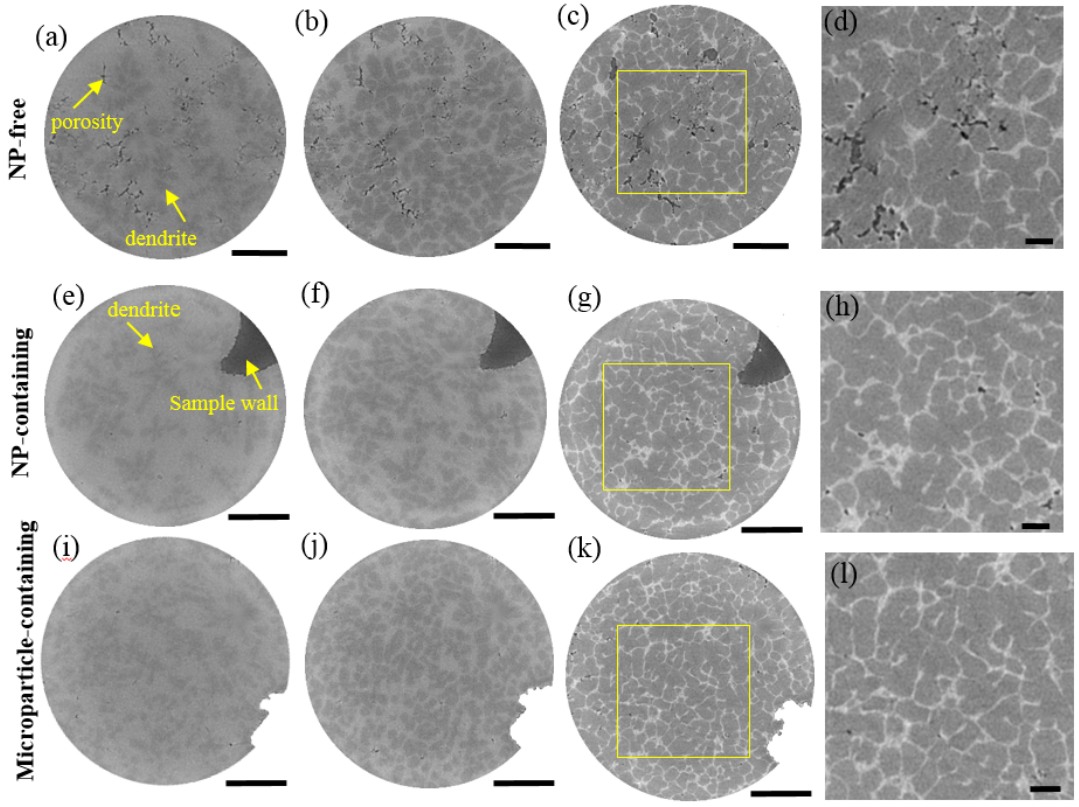

Fig. 2 Comparison of microstructures of Al-10wt.%Cu alloy solidified at 2 ºC/min: (a-d) without particles; (e-h) with ~1wt.% Al_2O_3 nanoparticles; (e-h) with ~1wt.% Al_2O_3 microparticles. Scale bar in each figure is 400 μm. (c), (g) and (f) are images after solidification, while (a-b, e-f, i-j) are images during solidification. (d), (h) and (l) are enlarged images of the area as indicated by rectangle in (c), (g) and (k), respectively.

3.2 3D dendritic evolution in Mg-25Zn-7Al alloys

In order to better examine the influence of NPs on the nucleation and dendritic growth, the 3D dendrites in the Mg-25Zn-7Al were further analyzed. Analysis of the 3D Al-10Cu grains will be presented in a future study. Fig. 3 shows the evolution in 3D of primary Mg dendrites, as seen from the lateral view, in the NP-free and NP-containing material during solidification at 3 ºC/min. Each dendritic grain is individually color rendered.

As can be seen in Fig. 3, compared to the NP-containing alloy, many fewer grains were initially observed to nucleate within the NP-free sample (i.e. 24 in Fig. 3(a) vs 109 in Fig. 3(d)). All these grains in the NP-free alloy nucleated on the surface of the sample wall, while grains in the NP-

containing alloy initially nucleated both on the sample surface and within the melt. Upon further cooling of 1.8 ºC, 14 more gains nucleated in the NP-free material (Fig. 3(b)), including 4 grains completely within the interior of the sample. These 4 dendrites nucleated on the surface of pre-existing pores within the melt. In comparison, 148 additional grains were observed upon further 1.8 ºC cooling (Fig. 3(e)) in the NP-containing sample and they nucleated throughout the sample. Only 3 more dendrites and 10 dendrites nucleated upon further cooling in the NP-free and NP-containing alloys, respectively. The quantitative results clearly show that the number of grains is significantly increased after the addition of NPs.

Fig. 4 further illustrates the degree to which nucleation occurred on the surface of the sample or within the melt through color-coding. As can be seen, there is a ring of grains that nucleate on the surface enclosing a few grains that nucleate within the centre. In the NP-free alloy all of the centre-nucleating grains nucleated on a pore or oxide. In the NP-containing alloy, ~5% of the grains nucleated directly in the liquid, without being in contact with a pore. Therefore, in both cases, nucleation on oxides or on the surface of the pre-existing pores is responsible for the main mechanism. In addition, the ultrasonic treatment may promote the dispersion of oxide pores within the melt and thus enabling the nucleation within the melt. However, the observation of ~5% grains directly nucleating from the melt without touching the pores still indicate that the SiC NPs (or their agglomeration) may have acted as nucleation site since SiC has been shown to be effective nuclei for the Mg-Al-Zn alloys [22-23].

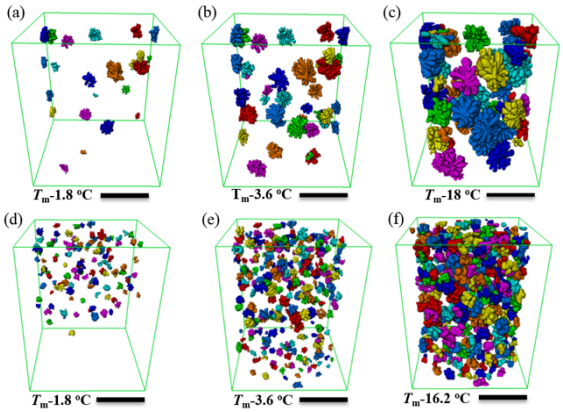

Fig. 3 Colour-rendered images showing the 3D grains of NP-free Mg-25Zn-7Al (a-c) and NP Mg-25Zn-7Al (d-f) during solidification at 3 ºC/min. Images were seen from lateral view. Scale bar equals 300 μm for all the images. The temperature was indicated under each figure. Note that the temperature variation for the indicated temperature is ~ 1.8 ºC.

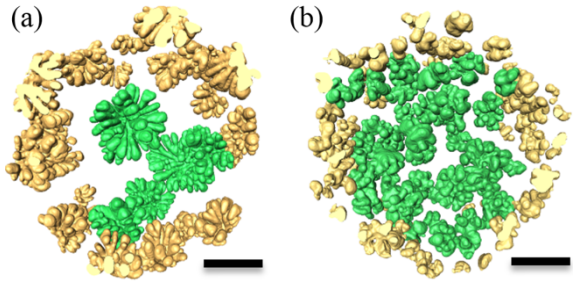

Fig. 4 Colour-rendered images showing the 3D grains of (a) NP-free Mg-25Zn-7Al and (b) NP Mg-25Zn-7Al alloys solidified at 3 ºC/min. Grains formed from sample wall and within sample are rendered in gold and green colour, respectively. The scale bar in each figure is 300 μm. The temperature was at T_m-12.6 ºC. After ref. [17] (E. Guo et al. Acta Mater. 2018).

The evolution of dendrite tip velocity was measured for each composition condition to evaluate the dendritic growth kinetics and to elucidate the influence of nanoparticles on the dendritic growth behavior. Fig. 5 shows the evolution of dendrite tip velocity in the NP-free and NP-containing Mg-25Zn-7Al alloy, along with the inset dendrites that were used for the measurement. A few branches were measured for each dendrite. A few features can be observed from the figure. First, the dendrites initially grew fast in an unconstrained growth mode when there was less interaction between the solute fields and the surrounding dendrites. Then, growth slowed down gradually due to the constraints imposed by solutal interactions with other dendrites ahead of the evolving solid/liquid interface. It is pointed out that Zn would dominate the growth restriction coefficient of the alloy because of its high content. Dendrites stopped growing once physical impingement occurred. Second, the dendritic tip velocity in the NP sample was lower than in the corresponding NP-free sample for the same cooling rate. Similar observation was made in previous study and was further supported by theoretical analyses that the densely packed NPs may block solute diffusion during solidification, and thus slow down the dendrite growth [24]. Third, the velocity of branches in the same dendrite varied from one to the other, depending on the spatial position of the branch relative to the other surrounding dendrites. It is pointed out that the initial growth velocity measured in this work represents a lower bound, as the scan time was too slow to capture the fast initial transients.

The inset images of two individual dendrites given in Fig. 5 show that the morphology of dendrites is different in the two alloys; the dendrite of the NP-free alloy exhibits a six-fold structure while the dendrite of the NP-containing alloy exhibits a more branched and spherical structure. We hypothesize that the transition from dendritic morphology to a hyper-branched/spherical structure

is a result of an increase in Zn content in the liquid ahead of the solid/liquid interface. Zn is known to modify the liquid/solid interface anisotropy [25] and further Zn diffusion is known to be greatly reduced in the presence of NPs in the liquid [24].

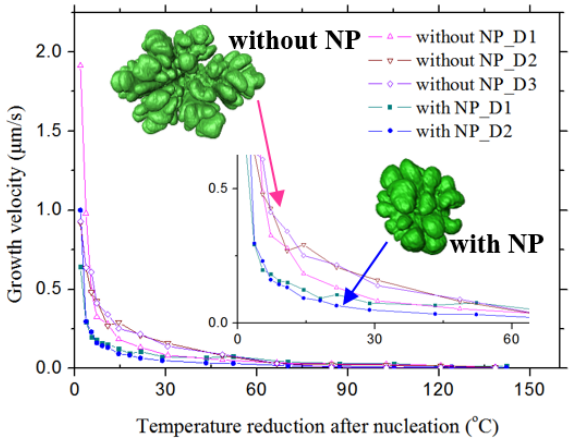

Fig. 5 Dendrite tip velocity for Mg-25Zn-7Al alloys solidified at 3 ºC/min (the inset graph shows a zoom of the larger dataset).

4. Conclusion

Using 4D synchrotron X-ray tomography, the evolving microstructure during solidification was characterized to investigate the influence of NPs on grain nucleation and dendritic growth dynamics in both magnesium and aluminum alloys. The detailed analyses of the 3D dendrites in the Mg-25Zn-7Al, including the number of grains formed in the sample and quantified results of dendrite tip velocity, lead to the following key findings:

(1) The addition of SiC NPs refines the grain structures of Mg-25Zn-7Al alloy due to a combination effect of increased grain nucleation and growth constraints imposed by the nanoparticles, while the Al_2O_3 particles, either nano or micron sized, are less effective in refining the Al grains in the Al-10Cu alloy.

(2) The dendritic morphology is modified in the NP-containing Mg-25Zn-7Al, changed from a six-fold structure to a hyper-branched structure with many splitting branches.

The results in this study demonstrate the ability of fast 4D tomography in revealing the mechanisms occurred when processing liquid MMNCs. The time evolved results also provide outstanding data for validating numerical studies of microstructural evolution.

Acknowledgement

E. Guo would like to thank the financial support from fundamental research funds for the central universities (grant No. DUT18RC(3)042).

Reference

[1] Daudin R, Terzi S, Lhuissier P, Tamayo J, Scheel M, Hari Babu N, Eskin DG, Salvo L (2017) Particle-induced morphological modification of Al alloy equiaxed dendrites revealed by sub-second in situ microtomography. Acta Mater. 125: 303-310.
[2] Wilde G, Byrnes M, Perepezko JH (1999) Particle-dendrite interaction during undercooled liquid solidification of metal matrix composites. J. Non-Cryst. Solids 250-252: 626-631.
[3] Chen XH, Yan H (2016) Solid-liquid interface dynamics during solidification of Al7075-Al2O3np based metal matrix composites. Mater. Des. 94: 148-158.
[4] Xu JQ, Chen LY, Choi H, Li XC (2012) Theoretical study and pathways for nanoparticle capture during solidification of metal melt. J. Phys-Condens. Mat. 24 (25): 255304.
[5] Watson IG, Forster MF, Lee PD, Dashwood RJ, Hamilton RW, Chirazi A (2005) Investigation of the clustering behaviour of titanium diboride particles in aluminium. Comp. A 36 (9): 1177-87.
[6] Watson IG, Lee PD, Dashwood R, Young P (2006) Simulation of the mechanical properties of an aluminum matrix composite using X-ray microtomography. Met. Trans. A 37: 551-558.
[7] Miracle DB (2005) Metal matrix composites – From science to technological significance. Comp. Sci. Technol. 65(15-16): 2526-2540.
[8] Sillekens WH, Jarvis DJ, Vorozhtsov A, Bojarevics V, Badini CF, Pavese M, Terzi S, Salvo L, Katsarou L, Dieringa H (2014) The ExoMet project: EU/ESA research on high-performance light-metal alloys and nanocomposites. Metall. Mater. Trans. A 45A (8): 3349-3361.
[9] Stjohn DJ, Easton MA, Qian M, Taylor JA (2013) Grain refinement of magnesium alloys: a review of recent research, theoretical developments, and their application. Metall, Mater. Trans. A 44A (7): 2935-2949.
[10] Wang DK, De Cicco MP, Li XC (2012) Using diluted master nanocomposites to achieve grain refinement and mechanical property enhancement in as-cast Al-9Mg. Mater. Sci. Eng. A 532: 396-400.
[11] Chawla N, Shen YL (2001) Mechanical behavior of particle reinforced metal matrix composites. Adv. Eng. Mater. 3 (6): 357-370.
[12] Shuai SS, Guo EY, Phillion AB, Callaghan MD, Jing T, Lee PD (2016) Fast synchrotron X-ray tomographic quantification of dendrite evolution during the solidification of Mg-Sn alloys. Acta Mater. 118: 260-269.
[13] Guo EY, Phillion AB, Cai B, Shuai SS, Kazantsev D, Jing T, Lee PD (2017) Dendritic evolution during coarsening of Mg-Zn alloys via 4D synchrotron tomography. Acta Mater. 123: 373-382.
[14] Daudin R, Terzi S, Lhuissier P, Salvo L, Boller E, Remelting and solidification of a 6082 Al alloy containing submicron yttria particles: 4D experimental study by in situ X-ray microtomography. Mater. Des. 87 (2015) 313-317.
[15] Karagadde K, Lee PD, Cai B, Fife JL, Azeem MA, Kareh KM, Puncreobutr C, Tsivoulas D, Connolley T, Atwood RC (2015) Transgranular liquation cracking of grains in the semi-solid state. Nat. Commun. 6: 8300.
[16] Daudin R, Terzi S, Lhuissier P, Tamayo J, Scheel M, Hari Babu N, Eskin DG, Salvo L (2017)

Particle-induced morphological modification of Al alloy equiaxed dendrites revealed by sub-second in situ microtomography. Acta Mater. 125: 303-310.
[17] Guo EY, Shuai SS, Kazantsev D, Karagadde S, Phillion AB, Jing T, Li WZ, Lee PD (2018) The influence of nanoparticles on dendritic grain growth in Mg alloys. Acta Mater. 152: 127-137.
[18] Kazantsev D, Guo E, Phillion AB, Withers PJ, Lee PD (2017) Model-based iterative reconstruction using higher-order regularization of dynamic synchrotron data. Meas. Sci. Technol., 28 (9): 094004.
[19] Quested TE, Greer AL (2005) A thermal heterogeneous nucleation of solidification. Acta Mater. 53: 2683-2692.
[20] Dieringa H (2018) Processing of magnesium-based metal matrix nanocomposites by ultrasound-assisted particle dispersion: A review. Metals 8(6): 431.
[21] Lee PD, Hunt JD (1997) Hydrogen porosity in directionally solidified aluminium-copper alloys: In-situ observation. Acta Mater. 45 (10): 4155-4169.
[22] Jia XY, Liu SY, Gao FP, Zhang QY, Li WZ (2009) Magnesium matrix nanocomposites fabricated by ultrasonic assisted casting. Int. J. Cast Metal Res. 22 (1-4): 196-199.
[23] Gunther R, Hartig C, Bormann R (2006) Grain refinement of AZ31 by (SiC)p: theoretical calculation and experiment. Acta Mater. 54 (20) 5591-5597.
[24] Chen LY, Xu JQ, Choi H, Konishi H, Jin S, Li XC (2014) Rapid control of phase growth by nanoparticles. Nat. Commun. 5: 3879.
[25] Shuai SS, Guo EY, Zheng QW, Wang MY, Jing T, Fu YN (2016) Three-dimensional a-Mg dendritic morphology and branching structure transition in Mg-Zn alloys. Mater. Charact. 118: 304-308.